Final Performance Report
Air Force Office of Scientific Research
Contract F49620-03-C-0019

Applying New Methods to Flare Prediction II: Realization of Methods for Photospheric Vector Magnetic Field Data and their Extension into the Chromosphere.

Dr. K.D. Leka, Principal Investigator
NorthWest Research Associates

March 2006

REPORT DOCUMENTATION PAGE

Form Approved
OMB No. 0704-0188

1. REPORT DATE *(DD-MM-YYYY)*	**2. REPORT TYPE**	**3. DATES COVERED** *(From - To)*
31-03-2006	Final Report	3/1/03 – 12/31/05

4. TITLE AND SUBTITLE

Applying New Methods for Photospheric Vector Magnetic Field Data and their Extension into the Chromosphere

5a. CONTRACT NUMBER
F49620-03-C-0019

5b. GRANT NUMBER

5c. PROGRAM ELEMENT NUMBER

6. AUTHOR(S)

K.D. Leka

5d. PROJECT NUMBER

5e. TASK NUMBER

5f. WORK UNIT NUMBER

7. PERFORMING ORGANIZATION NAME(S) AND ADDRESS(ES)

NorthWest Research Associates
14508 NE 20th St.
PO Box 3027
Bellevue, WA 98009-3027

8. PERFORMING ORGANIZATION REPORT NUMBER
NWRA-BELL-06-R321

9. SPONSORING / MONITORING AGENCY NAME(S) AND ADDRESS(ES)

Air Force Office of Scientific Research
Attn: Major David L. Byers
4015 Wilson Blvd., Rm 713
Arlington, VA 22203-1954

10. SPONSOR/MONITOR'S ACRONYM(S)

11. SPONSOR/MONITOR'S REPORT NUMBER(S) AFRL-SR-AR-TR-06-0152

12. DISTRIBUTION / AVAILABILITY STATEMENT **Distribution A: Approved for Public Release**

13. SUPPLEMENTARY NOTES

14. ABSTRACT

The goals for this AFOSR contract focused on analysis and interpretation of solar magnetic field data in the context of solar flare prediction. Drs. Leka (P.I), Barnes and Metcalf (with collaborators) have been productive in all respects; our quantitative, physics-based statistical approaches are gaining wide recognition and proving quite powerful. We showed that using daily magnetograms produces forecasts which compare favorably to those from NOAA. However, unless temporal evolution is explicitly observed and considered, the daily results provide limited value-added to a null or "no flare" forecast. Time-series photospheric data may distinguish flare-imminent from flare-quiet epochs, and when such data are used to model and parameterize the evolving coronal magnetic topology, forecast performance may improve considerably. The plausibility that the magnetic kink instability is a trigger mechanism for energetic events was re-examined using a new and more solar-appropriate technique for measuring the twist in solar magnetic fields. Finally, acquisition and interpretation of chromospheric magnetic field data continued, including direct measure of the magnetic free energy in super active-region NOAA 10486. Throughout, we maintained high visibility within the technical community, with 8 published/submitted papers, 3 anticipated, 13 invited seminars, and over twenty other interactions including contributions to professional meetings.

15. SUBJECT TERMS

16. SECURITY CLASSIFICATION OF:			**17. LIMITATION OF ABSTRACT**	**18. NUMBER OF PAGES**	**19a. NAME OF RESPONSIBLE PERSON**
a. REPORT	**b. ABSTRACT**	**c. THIS PAGE**		28	**19b. TELEPHONE NUMBER** *(include area code)*

Contents

1 Summary of Effort **1**

2 Accomplishments: Research Highlights **2**
1 The Photospheric Magnetic Field Properties of Flaring vs. Flare-Quiet Active Regions, Initial Results . . . 2
2 Do Solar Active Regions Contain Sufficient Twist to be Kink Unstable? . . . 3
1 Summary . . . 4
3 Quantifying the Coronal Magnetic Topology of Solar Active Regions . . . 4
1 What is Magnetic Charge Topology? . . . 5
2 Applying MCT models to Observations . . . 5
4 The Coronal Magnetic Topology as related to Solar Flares . . . 7
1 Summary of Analysis . . . 7
5 Analysis of a Statistically Significant Sample of Daily Magnetograms . . . 10
1 The Database and Analysis . . . 11
2 Summary of Results . . . 11
6 Probabilistic Forecasts from Daily Vector Magnetograms . . . 13
1 Summary of Results . . . 13
7 Spectropolarimetry and Magnetic Field Maps in the Chromosphere . . . 15
8 Measuring the Free Magnetic Energy in Solar Active Regions . . . 16
1 The Free Magnetic Energy of Super Active-Region 10486 . . . 16
2 Improving the Algorithm for Measuring the Free Energy . . . 16
3 Free Energy as Statistically Related to Solar Flare Productivity . . . 17

3 References **18**

4 Accomplishments: Technical Highlights **20**
1 Discriminant Analysis . . . 20
2 Magnetic Field Analysis . . . 20
3 Partitioning and the Coronal Topology for Time-Series Data . . . 21
4 Data Reduction and Inversion of Chromospheric Spectropolarimetry . . . 21

5 Additional Summaries **21**
1 Significance to the Technical Field . . . 21
2 Relationship to Original Goals . . . 22
3 Relevance to the Air Force Mission . . . 22
4 Potential Applications to Technology Challenges . . . 23
5 Personnel Supported . . . 23
6 Publications Citing this AFOSR Support (current and anticipated): . . . 23
7 Interactions: . . . 24
1 Invited Lectures and Presentations: . . . 24
2 Consultative and Advisory Functions: . . . 25
3 Participation in and Presentations at Professional Meetings: . . . 25
4 Extended Scientific Visits to and From Other Laboratories . . . 27
5 Professional Activities (editorships, conference and society committees, *etc.*) . 27

6 Appendix **28**

List of Figures

1 Partitioning and locations of nulls and separators for NOAA AR 8210 6
2 Example discriminant function for MCT parameters based on time-series data 10
3 Example discriminant functions based on a statistically significant number of daily magnetograms. 12
4 Reliability plot for DA forecast. 14
5 Magnetic free energy of active regions 17

List of Tables

1 Parameters used in the discriminant analysis 8
1 – Continued 9
2 Classification Table for $d\sigma(X_i)/dt$, $d\varsigma(l)/dt$ 10
3 Comparison of Verification Statistics for DA method with the SEC and Bayesian (37) Methods 14

1 Summary of Effort

The tasks set forth for this contract focused on the analysis of solar magnetic field data and its interpretation in the context of solar flare prediction. Our approaches have been quantitative, statistical, and physics-based, using data from the solar photosphere. We supplemented the approach with an investigation into using magnetic field data from the solar chromosphere, where it is believed that the measurements will yield more about the relevant physical process than can be inferred using solely photospheric data. The following achievements are noted:

1. An analysis of time-series solar photospheric vector magnetic field data comparing the evolution prior to solar flare events to event-quiet times, demonstrating that unique flare-predictors were rare (17) .

2. The introduction of a statistical analysis method, Discriminant Analysis, to the question of differentiating flare-imminent from flare-quiet times again using time-series of vector field data (18).

3. The application of a Magnetic Charge Topology model to time-series vector field data to characterize the coronal magnetic topology and its temporal variations (4).

4. A coupling of the MCT analysis of time-series data and Discriminant Analysis, demonstrating that modeling the solar corona may provide more information than the photosphere concerning whether the solar atmosphere is in a flare-imminent state (2).

5. A further application of Discriminant Analysis to a statistically-significant (over 1,200) sample of daily vector magnetograms, with discussions on the limitations of "snapshot" (rather than time-series) data for flare-prediction, and on non-parametric approaches (19).

6. A comparison of the resulting "daily forecast" capability to those produced by both the NOAA/Space Environment Center and by a new Baysian approach (3).

7. A demonstration that a common method used to infer the degree of "twist" in solar active regions using photospheric vector field data can systematically underestimate the magnetic helicity. A new method was proposed that relies upon more solar-appropriate assumptions and was shown to reproduce the known helicity in a model field (20).

8. The data reduction and analysis procedures were refined and described for obtaining chromospheric magnetograms from NaI spectropolarimetry data of the Imaging Vector Magnetograph (27).

9. The magnetic free energy of super active region NOAA 10486 was evaluated using chromospheric magnetograms, showing that it indeed contained enough free energy to produce the record-breaking events (26).

10. An investigation of the relation between the magnetic free energy of a variety of active regions and their productivity of energetic events (22).

2 Accomplishments: Research Highlights

This has been a productive research effort. The goal was to investigate methods relevant to solar flare prediction, and we developed numerous analysis methods and described both their potential and their limitations in the generally-accessible scientific literature. Below are summaries of the research efforts we undertook during the period of this contract.

2.1 The Photospheric Magnetic Field Properties of Flaring vs. Flare-Quiet Active Regions, Initial Results

The primary results of the previous contract, F49620-00-C-0004, K. D. Leka Principal Investigator, were submitted at the time that contract's final task report was submitted, and published during the period of performance of this contract. The goal was to develop a quantitative analysis of solar photospheric vector magnetic field data in the context of distinguishing what observable quantity, if any, could foretell an imminent solar flare.

Leka, K.D. and Barnes, G. 2003, "Photospheric Magnetic Field Properties of Flaring versus Flare-Quiet Active Regions. I. Data, General Approach, and Sample Results", *Astrophys. J.*, **595**, 1277.

Abstract

Photospheric vector magnetic field data from the U. Hawai'i Imaging Vector Magnetograph with good spatial and temporal sampling, are used to study the question of identifying a pre-flare signature unique to flare events in parameters derived from $\boldsymbol{B}$. In this first of a series of papers, we present the data analysis procedure and sample results focusing only on three active regions (NOAA Active Regions #8636, #8891, and #0030), three flares (two M-class and one X-class), and (most importantly) a flare-quiet epoch in a comparable flare-producing region. Quantities such as the distribution of the field morphology, horizontal spatial gradients of the field, vertical current, current helicity, "twist" parameter α and magnetic shear angles are parameterized using their moments and appropriate summations. The time series of the resulting parameterizations are examined one at a time for systematic differences in overall magnitude and evolution between the flare and flare-quiet examples. The variations expected due to atmospheric seeing changes are explicitly included. In this qualitative approach we find (1) no obvious flare-imminent signatures from the plain magnetic field vector and higher moments of its horizontal gradient, or from most parameterizations of the vertical current density; (2) counter-intuitive but distinct flare-quiet implications from the inclination angle, and higher moments of the photospheric excess magnetic energy; (3) flare-specific or flare-productivity signatures, sometimes weak, from the lower moments of the field gradients, kurtosis of the vertical current density, magnetic twist, current helicity density and magnetic shear angle. The strongest results are, however, that (4) in ensuring a flare-unique signature, numerous candidate parameters (considering both their variation and overall magnitude) are nullified on account of similar behavior in a flare-quiet region, and hence (5) considering single parameters at a time in this qualitative manner is inadequate. To address these limitations, a quantitative statistical approach is presented in Paper II (18).

Leka, K.D. and Barnes, G. 2003, "Photospheric Magnetic Field Properties of Flaring Versus Flare-Quiet Active Regions. II. Discriminant Analysis", *Astrophys. J.*, **595**, 1296.

Abstract

We apply statistical tests based upon discriminant analysis to the wide range of photospheric magnetic parameters described in Paper I (17), with the goal of identifying those properties which are important for the production of energetic events such as solar flares. The photospheric vector magnetic field data from the U. Hawai'i Imaging Vector Magnetograph are well-sampled both temporally and spatially, and we include here data covering 24 flare-event and flare-quiet epochs taken from seven active regions. The mean value and rate of change of each magnetic parameter are treated as separate variables, thus evaluating both the parameter's state and its evolution, to determine which properties are associated with flaring. Considering single variables first, Hotelling's T^2-tests show small statistical differences between flare-producing and flare-quiet epochs. Even pairs of variables considered simultaneously, which do show statistical difference for a number of properties, have high error rates, implying a large degree of overlap of the samples. To better distinguish between flare-producing and flare-quiet populations, larger numbers of variables are simultaneously considered; lower error rates result, but no unique combination of variables is clearly the best discriminator. The sample size is too small to directly compare the predictive power of large numbers of variables simultaneously. Instead, we rank all possible four-variable permutations based on Hotelling's T^2-test, and look for the most frequently appearing variables in the best permutations, with the interpretation that they are most likely to be associated with flaring. These variables include: an increasing kurtosis of the twist parameter, a larger standard deviation of the twist parameter, but a smaller standard deviation of the distribution of the horizontal shear angle and of the distribution of the horizontal magnetic field, but a larger kurtosis of that horizontal field. To support the "sorting all permutations" method of selecting the most frequently occurring variables, we show that the results of a single ten-variable discriminant analysis are consistent with the ranking. We demonstrate that individually, the variables considered here have little ability to differentiate between flaring and flare-quiet populations, but with multi-variable combinations, the populations may be distinguished.

With a quantitative approach including a comparison of flaring and flare-quiet epochs, these studies have earned respectable citation indicies in a very short time. They also began the series of papers we have built on during the present contract period.

2.2 Do Solar Active Regions Contain Sufficient Twist to be Kink Unstable?

Leka, K.D., Fan, Y. and Barnes, G. 2005, "On the Availability of Sufficient Twist to Trigger the Kink Instability", *Astrophys. J.*, **626**, 1091.

Abstract

The question of whether there is sufficient magnetic twist in solar active regions for the onset of the kink instability is examined using a blind test of analysis methods commonly used to interpret observational data. Photospheric magnetograms are constructed from a recently developed numerical simulation of a kink-unstable emerging flux rope with nearly constant (negative) wind. The calculation of the best-fit linear force-free parameter $\alpha_{\rm best}$ is applied, with the goal of recovering the model input helicity. It is shown that for this simple magnetic structure, three effects combine to produce an underestimation of the known helicity: (1) the influence of horizontal fields with lower local values within the flux rope; (2) an assumed simple relation between best and the winding rate q does not apply to non-axis fields in a flux rope that is not thin; and (3) the difficulty in interpreting the force-free twist parameter measured

for a field that is *forced*. A different method to evaluate the magnetic twist in active region flux ropes is presented, which is based on evaluating the peak α value at the flux rope axis. When applied to data from the numerical simulation, the twist component of the magnetic helicity is essentially recovered. Both the $\alpha_{\rm best}$ and the new $\alpha_{\rm peak}$ methods are then applied to observational photospheric vector magnetic field data of NOAA AR 7201. The $\alpha_{\rm best}$ approach is then confounded further in NOAA AR 7201 by a distribution that contains both signs, as is generally observed in active regions. The result from the proposed $\alpha_{\rm peak}$ approach suggests that a larger magnetic twist is present in this active region's δ-spot than would have been inferred from $\alpha_{\rm best}$ by at least a factor of 3. It is argued that the magnetic fields in localized active region flux ropes may indeed carry great than 2π winds and thus the kink instability is a possible trigger mechanism for solar flares and coronal mass ejections.

2.2.1 Summary

It has been argued (16) that there is insufficient twist present in any active region for the kink instability to be important in triggering solar eruptive events. We have shown that the analysis leading to this conclusion is incorrect on a variety of levels, and thus that the kink instability is still a candidate as the cause of flares and coronal mass ejections. The stability criterion for the onset of the kink mode is typically expressed in terms of the rate at which field lines wind about the axis of a flux tube. This quantity, q, is only simply related to the force-free parameter, α on the axis of a flux tube. The calculated value for α (16; 32), assigns a single value $\alpha_{\rm best}$ to characterize an entire active region, rather than the value of α on the axis of a flux rope. Since typical active regions contain flux ropes with both signs of the force-free parameter, $\alpha_{\rm best}$ generally greatly underestimates the rate of winding for any particular flux tube, and hence underestimates the amount of twist present. It was shown that even determining $\alpha_{\rm best}$ for an isolated flux tube typically results in a value significantly lower than the value on the axis of the flux tube. Further, the force-free parameter is only meaningful when the magnetic field is force-free, which is generally not the case for the photospheric observations.

We proposed a new approach, which uses the peak value of the force-free parameter as an estimate for α on the axis. For the analytic Gold & Hoyle solution (8), the new method correctly determines the rate of wind. To confirm our analysis, our approach, along with the approach of (16) was applied to an MHD simulation of a rising flux tube (7) for which the helicity, and hence the total twist, could be calculated by direct integration of the appropriate fields and vector potentials. The $\alpha_{\rm peak}$ method was successful in recovering the twist in the simulation, while the $\alpha_{\rm best}$ approach underestimated it by at least a factor of three. Finally, the new $\alpha_{\rm peak}$ approach was applied to an active region containing an emerging flux region in which it was straightforward to identify the footpoints of a single flux tube. Contrary to the earlier findings (16), we inferred a twist that was close to the stability limit for this active region.

2.3 Quantifying the Coronal Magnetic Topology of Solar Active Regions

Barnes, G., Longcope, D. and Leka, K.D. 2005, "Implementing a Magnetic Charge Topology Model for Solar Active Regions", *Astrophys. J.*, **629**, 561.

Abstract

Information about the magnetic topology of the solar corona is crucial to the understanding of solar energetic events. One approach to characterizing the topology that has had some success is magnetic charge topology, in which the topology is defined by partitioning the observed photospheric field into a set of discrete sources and determining which pairs are interlinked by

coronal field lines. The level of topological activity is then quantified through the transfer of flux between regions of differing field line connectivity. We discuss in detail how to implement such a model for a time series of vector magnetograms, paying particular attention to distinguishing real evolution of the photospheric magnetic flux from changes due to variations in atmospheric seeing, as well as uncorrelated noise. We determine the reliability of our method and estimate the uncertainties in its results. We then demonstrate it through an application to NOAA active region 8210, which has been the subject of extensive previous study.

2.3.1 What is Magnetic Charge Topology?

Although it is generally accepted that solar flares occur through the release of energy stored in the coronal magnetic field, it is still not clear what initiates this release. Theoretical considerations indicate that magnetic reconnection is likely to play a role in either the initiation of a flare or in the energy release. From this hypothesis it would seem that modeling reconnection is crucial to understanding flares. One class of models for reconnection is Magnetic Charge Topology (5; 9; 33; 15; 6; 31). MCT models assume that the photospheric magnetic field consists of distinct concentrations of magnetic flux, presumably the manifestations of sub-photospheric flux tubes, and represent each concentration by a source or "charge".

With a few special exceptions, every field line in this configuration must start on a source and end on source of the opposite polarity. Bundles of field lines connecting the same pair of sources neatly divide the corona into distinct flux domains. Each flux domain is enclosed by a separatrix surface, which is composed of field lines that have one end on a magnetic null point, where the field vanishes. The intersection of separatrices is a separator field line, which begins and ends on null points. In this simplified context, magnetic reconnection occurs when a pair of field lines exchange footpoints, which is equivalent to transporting flux from one domain to another. Such an exchange occurs across a separator field line. Thus the location of separator field lines provides insight into the possible locations for reconnection, and the heating which is likely to accompany rapid reconnection.

2.3.2 Applying MCT models to Observations

In order to apply MCT models to observations, photospheric fields must somehow be represented as a set of distinct sources. This partitioning is motivated by the well-known tendency of photospheric flux to concentrate, albeit not always into completely distinct regions. We have developed a robust algorithm for partitioning the field in a long time series of vector magnetograms of solar active regions. The emphasis in the approach is to distinguish real changes in the concentrations from changes due to uncorrelated noise and variations in atmospheric seeing.

The main challenge in applying this approach to real time series of data is that systematic and random noise can cause apparent changes in the concentrations of flux. To mitigate this issue, the approach we developed starts by constructing a reference magnetogram, consisting of the time averaged vertical field at each co-aligned pixel in the time series. Source regions in the reference magnetogram are defined by propagating "region labels" downhill from local maxima in $|B_z|$, until each pixel is associated with a local maximum (34). This can result in an excessively large number of small partitions in regions of plage, which we believe are not important to solar flares; thus we simplify the resulting partitions by merging neighboring regions if the vertical field strength at the saddle point between the regions is within 100 G of the maximum field strength of either region. Once the reference magnetogram has been partitioned, all the magnetograms in the time series are partitioned by minimizing their differences from the reference partition. The resulting partitions

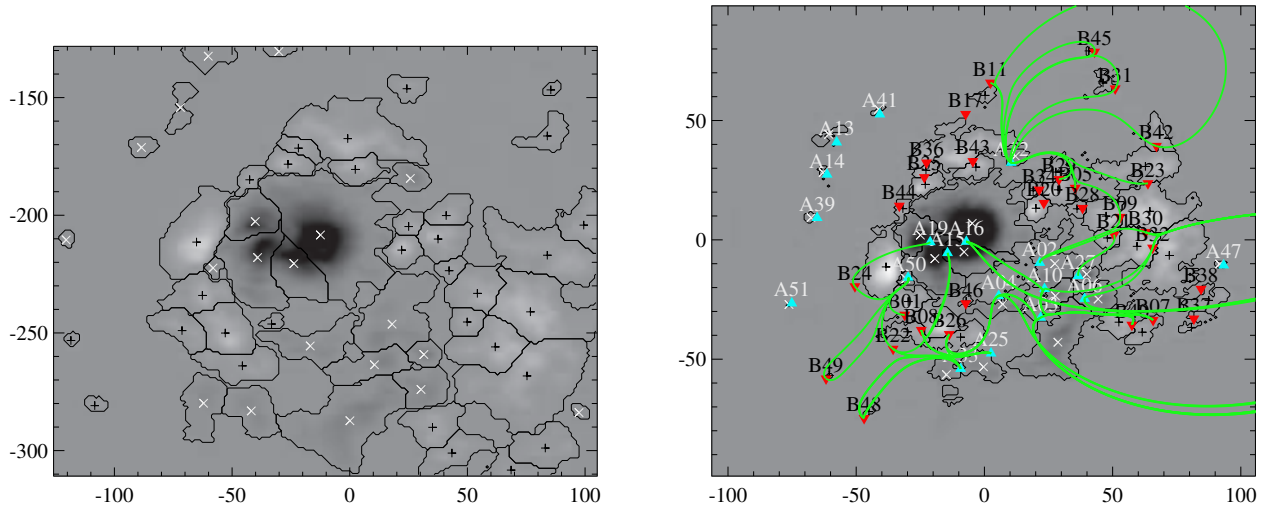

Figure 1: NOAA AR 8210 on 1998 May 01. **Left:** Reference magnetogram for NOAA AR 8210, showing the time averaged vertical field, the 52 partitions and the pole locations. Note that our partitioning algorithm retains the divisions between strong flux concentrations in the large negative polarity sunspot, and the small positive polarity intrusion located at $(x, y) \approx (-35, -245)$ while significantly simplifying the large areas of plage. **Right:** Magnetogram showing the vertical field (greyscale), the partitions (contours), the locations of the sources (+ and × for positive and negative) and nulls (blue for A-type, red for B-type), and the projection of the separators onto the photosphere (green lines). Adapted from (4).

tend to persist through the entire time series, thus presumably representing the true concentrations of photospheric magnetic flux. Figure 1 (left) shows the reference magnetogram and partitioning for NOAA AR 8210, compared to the partitioning for one magnetogram from the time series (Figure 1, right, in heliographic coordinates). The exact boundaries of the partitions have changed, but all the partitions present in the reference are also present in the example time.

Once a magnetogram has been partitioned, the topological properties of the coronal field can be determined. The domain matrix, representing the flux connecting each pair of sources, is determined by tracing magnetic field lines then using a Bayesian estimate for the flux based on the number of field lines connecting each pair of sources:

$$\psi_{ij} \quad = \quad \frac{m_{ij} + m_{ji}}{N_i/\Phi_i + N_j/\Phi_j} \tag{1}$$

where m_{ij} is the number of field lines connecting source i to source j, N_i is the total number of field lines initiated from source i, and Φ_i is the flux of source i. Using a total of 2.5×10^7 field lines for NOAA AR 8210 allows us to locate domains down to a size $\psi_c \approx 0.15\,\mathrm{G\,Mm^2}$, which is likely to be far less than needed for understanding solar flares. The magnetic null points are located using a Newton-Raphson root-finding algorithm, initiated at locations determined by considering pairs and triplets of sources in isolation. The null points found in NOAA AR 8210 satisfy both the Poincaré indices (23, see), thus it is likely that all null points have been located. The first step in locating the separators is to determine which nulls are linked. We trace field lines initiated at a range of angles in the fan surface of each null point. When the field lines end on different sources, at least one separator must be bracketed by the field lines, and the null from which the field lines were initiated must be linked to another null associated with the pair of sources. The existence of a separator between a pair of linked nulls is confirmed by considering the intersection of the

four bracketing field lines with a plane midway between the nulls. Knowledge of the sources, nulls, domain matrix and separatrices quantifies the coronal topology at each time.

2.4 The Coronal Magnetic Topology as related to Solar Flares

Barnes, G., and Leka, K.D. 2006, "Photospheric Magnetic Field Properties of Flaring Versus Flare-Quiet Active Regions III: Magnetic Charge Topology Models", *Astrophys. J.*, submitted.

Abstract

A Magnetic Charge Topology (MCT) model is applied to time series of photospheric vector magnetic field data for seven active regions divided into epochs classified as flare-quiet and flare-productive. In an approach which parallels an earlier study by the authors using quantities describing the photospheric properties of the vector magnetic field, we define quantities derived from the MCT analysis that quantify the complexity and topology of the active region coronal fields. With the goal of distinguishing between flare-quiet and flare-imminent magnetic topology, the time series are initially displayed for three active regions for visual inspection with few clear distinguishing characteristics resulting. However, an analysis of all twenty-four epochs using the Discriminant Analysis statistical approach indicates that coronal field topology, derived from observed photospheric vertical field, may indeed hold relevant information for distinguishing these populations, although the small sample size precludes a definite conclusion. The variables derived from the characterization of coronal topology routinely result in higher probabilities of being able to distinguish between the two populations than the analogous variables derived for the photospheric field.

2.4.1 Summary of Analysis

Having determined how to implement this MCT model for solar active regions, we investigated the relationship between coronal magnetic topology and flaring using discriminant analysis. MCT analysis was applied to the data set developed under our previous AFOSR contract, consisting of 24 epochs from seven different active regions, including 10 flaring epochs. A broad spectrum of parameters describing the coronal topology was computed, as listed in Table 1. The parameters cover four broad categories of the topology: the sources, the domain matrix, the null points and the separators. In each case, the detailed distribution of the parameters is represented by its first four moments.

Table 1: Parameters used in the discriminant analysis

variable	description
S	number of sources
	Distribution of Source Flux
$\overline{\Phi_i}$	mean of source flux
$\sigma(\Phi_i B_z)$	standard deviation of source flux
$\varsigma(\Phi_i B_z)$	skew of source flux
$\kappa(\Phi_i B_z)$	kurtosis of source flux
$E_B = \sum_{i<j} q_i q_j / \lvert \boldsymbol{x}_i - \boldsymbol{x}_j \rvert$	magnetostatic energy
	Distribution of Connectivity
$\overline{C_i}$	mean number of connections per pole
$\sigma(C_i)$	standard deviation of number of connections per pole
$\varsigma(C_i)$	skew of number of connections per pole
$\kappa(C_i)$	kurtosis of number of connections per pole
$C = \sum C_i$	total number of connections
C_∞	number of connections to infinity
	Distribution of Domain Flux
$\overline{\psi_{ij}}$	mean flux in each connection
$\sigma(\psi_{ij})$	standard deviation of flux in each connection
$\varsigma(\psi_{ij})$	skew of flux in each connection
$\kappa(\psi_{ij})$	kurtosis of flux in each connection
	Distribution of Flux Weighted Distance
$\overline{\lvert \boldsymbol{x}_i - \boldsymbol{x}_j \rvert}$	mean flux weighted distance
$\sigma(\lvert \boldsymbol{x}_i - \boldsymbol{x}_j \rvert)$	standard deviation of flux weighted distance
$\varsigma(\lvert \boldsymbol{x}_i - \boldsymbol{x}_j \rvert)$	skew of flux weighted distance
$\kappa(\lvert \boldsymbol{x}_i - \boldsymbol{x}_j \rvert)$	kurtosis of flux weighted distance
	Distribution of Flux per Distance
flux per distance	$\phi_{ij} = \psi_{ij} / \lvert \boldsymbol{x}_i - \boldsymbol{x}_j \rvert$
$\overline{\phi_{ij}}$	mean flux per distance
$\sigma(\phi_{ij})$	standard deviation of flux per distance
$\varsigma(\phi_{ij})$	skew of flux per distance
$\kappa(\phi_{ij})$	kurtosis of flux per distance
$\phi_{\mathrm{tot}} = \sum \phi_{ij}$	total flux per distance
	Distribution of Tilt Angle
tilt angle	$\xi_{ij} = \tan^{-1}[(y_j - y_i)/(x_j - x_i)]$
$\overline{\xi_{ij}}$	mean flux weighted tilt angle
$\sigma(\xi_{ij})$	standard deviation of flux weighted tilt angle
$\varsigma(\xi_{ij})$	skew of flux weighted tilt angle
$\kappa(\xi_{ij})$	kurtosis of flux weighted tilt angle
	Number of Nulls
N_{p0}	number of prone nulls
N_{u0}	number of upright nulls
	Distribution of Number of Separators
$\overline{X_i}$	mean number of separators per null
$\sigma(X_i)$	standard deviation of number of separators per null
$\varsigma(X_i)$	skew of number of separators per null
$\kappa(X_i)$	kurtosis of number of separators per null
$X = \sum X_i$	total number of separators

Table 1: – Continued

variable	description
	Distribution of Length of Separators
$\overline{l_i}$	mean length of separators
$\sigma(l_i)$	standard deviation of length of separators
$\varsigma(l_i)$	skew of length of separators
$\kappa(l_i)$	kurtosis of length of separators
	Distribution of Flux Enclosed by Separators
flux enclosed	$\Psi_i = \oint \boldsymbol{A} \cdot d\boldsymbol{l}$
$\overline{\lvert\Psi_i\rvert}$	mean unsigned flux enclosed by separators
$\sigma(\lvert\Psi_i\rvert)$	standard deviation of unsigned flux enclosed by separators
$\varsigma(\lvert\Psi_i\rvert)$	skew of unsigned flux enclosed by separators
$\kappa(\lvert\Psi_i\rvert)$	kurtosis of unsigned flux enclosed by separators
$\lvert\Psi_{\rm tot}\rvert = \sum \lvert\Psi_i\rvert$	total unsigned flux enclosed by separators
	Distribution of Maximum Height of Separators
$\overline{z_i}$	mean maximum height above photosphere
$\sigma(z_i)$	standard deviation of maximum height above photosphere
$\varsigma(z_i)$	skew of maximum height above photosphere
$\kappa(z_i)$	kurtosis of maximum height above photosphere
	Number of Multiple Domains
L	number of pairs of nulls with multiple separators
$D_m = X + S - 1 - C$	number of extra domains
For each of these parameters, we consider the mean value for an epoch, denoted by $\langle\rangle$ and the slope of a regression line, denoted by d/dt.	

Consideration of individual parameters for a few selected regions produces ambiguous results, as with photospheric analysis (17). To examine how the topology may relate to flaring, we turn again to a statistical approach that simultaneously considers multiple variables: Discriminant Analysis (e.g., 11; 1). Parameter space is divided into two regions, such that measurements from a new epoch which fall in one of the regions are predicted to flare, while measurements which fall in the other region are predicted to be flare quiet. The boundary between the two regions is constructed so as to maximize the overall rate of correct predictions. Under the assumptions described in (18), including that the population distributions are Gaussian with equal covariance matrices, the boundary is a hyperplane which simply reduces to a line in two dimensions.

As a demonstration of discriminant analysis, we show in Figure 2 the best combination of two variables derived from the MCT analysis: the slope of the standard deviation of the distribution of the number of separators on each null versus the slope of the skew of the distribution of separator lengths. The mean of the flaring population has an increasing $d\sigma(X_i)/dt$ but a decreasing $d\varsigma(l_i)/dt$ implying that in the flaring regions the lengths of separators were becoming more homogeneous while the distribution of them amongst nulls was in fact becoming less so. This pair correctly classifies 87.5% of the points (Table 2), which is significantly better than any 2-variable pair using the photospheric parameters (18). It also returns a probability that the samples indeed represent two different populations of 0.974, compared to 0.943 from the best photospheric 2-variable combination.

We caution that this is a demonstration only, with far fewer data points than adequate for a robust interpretation, but it appears that *characterizing the coronal magnetic topology is a better approach to flare forecasting than characterizing the photospheric magnetic field.*

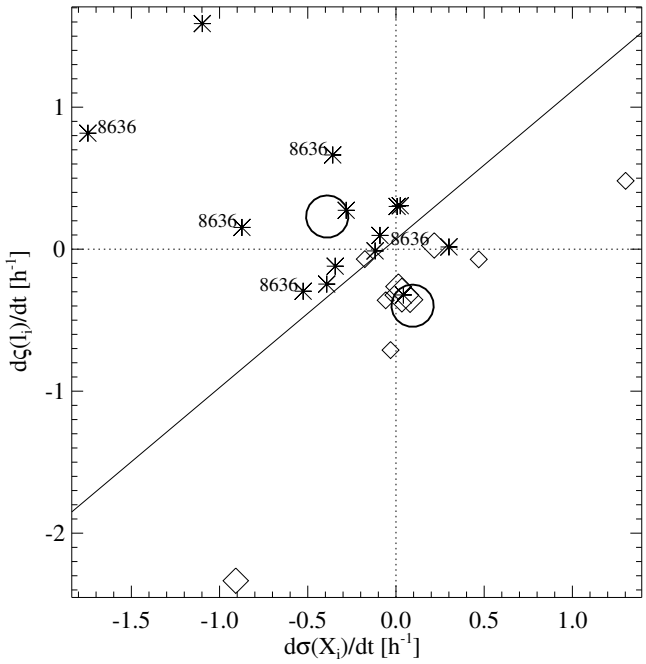

Figure 2: The discriminant function for the variables $d\sigma(X_i)/dt$, $d\varsigma(l_i)/dt$. Diamonds indicate flaring epochs and are sized by the flare class, with the smallest being C-class, intermediate being M-class, and the largest being X-class; asterisks indicate quiet epochs. The discriminant function is the solid line, and the means of each sample are indicated by large circles. A new epoch that falls below and to the right of the line would be forecast to flare, while one above and to the left of the line would be forecast to be flare-quiet. One active region (AR 8636) has been labeled to give an indication of the amount of scatter between epochs.

Table 2: Classification Table for $d\sigma(X_i)/dt$, $d\varsigma(l)/dt$

		predicted	
		flare	no flare
observed	flare	9	1
	no flare	2	12

2.5 Analysis of a Statistically Significant Sample of Daily Magnetograms

Leka, K.D. and Barnes, G. 2006, "Photospheric Magnetic Field Properties of Flaring Versus Flare-Quiet Active Regions IV: Discriminant Analysis of a Statistically Significant Sample of Daily Photospheric Magnetograms", *Astrophys. J.*, to be submitted.

Abstract

We apply statistical tests based on discriminant analysis to a subset of the photospheric magnetic parameters described in previous papers in this series, with the same goal of identifying those properties that are important for the production of energetic events such as solar flares. The photospheric vector magnetic field data are the U. Hawai'i Imaging Vector Magnetograph daily "survey" magnetograms of numbered active regions on the solar disk for the days on which observations were available from January 2001 to December 2004. The resulting 1212 magnetograms include 359 regions which produced at least one C-flare in the 24 hour period

following the observation. We show that the same variables tend to emerge as important in distinguishing a flare imminent active region whether the selection criterion is an estimate of the error rate of the discriminant function, or is the probability that the flaring and flare-quiet samples come from different populations. Considering multiple variables simultaneously indicates that a combination of only a few variables is able to encompass almost all the predictive power of the photospheric parameters, but the choice of which few variables is not unique due to strong correlations among the variables. In particular, we find that the total magnetic flux, the total vertical current, the total vertical component of the heterogeneity current, and estimates of the total current helicity and excess photospheric magnetic energy are strongly correlated, and are some of the most powerful predictors. The best discriminant functions result from combining one of these variables with other uncorrelated variables, such as measures of the magnetic shear along neutral lines. The best combinations successfully classify over 80% of the regions, however this is a relatively modest improvement over the success rate of approximately 70% achieved by classifying all regions as flare quiet. Thus we conclude that the state of the photospheric magnetic field at any given time has limited bearing on whether a flare is imminent. Our results are based on linear discriminant analysis, but we demonstrate, using nonparametric estimates of the probability density functions, that the conclusions are quite robust.

2.5.1 The Database and Analysis

For this study, we make use of a different data set, consisting of daily snapshots taken by the IVM of each numbered active region on the disk. This precludes considering the temporal evolution of the photospheric field beyond gross daily changes, which we do not consider. Nonetheless, this approach allows us to draw conclusions from a statistically significant sample, and to make daily forecasts against which to compare NOAA's predictions.

The data source for this project is the archive of "survey" data acquired by the IVM, whereby each visible numbered active region is the target for a single magnetogram at the beginning of each observing day. The magnetograms were reduced using a "quick-look" algorithm but otherwise were handled analogously to the time-series data, undergoing the ambiguity-resolution and variable calculations. Magnetograms for active regions at extreme observing angles and those with only very weak fields ($< 2\sigma$, *i.e.,* active regions with weak plage only), were excluded; however, no additional selection rules were imposed. From the years 2001–2004, over 1,200 magnetograms comprise the final database.

Each observed photospheric magnetic field is parametrized in the same fashion as previously (17; 18), with moments of the distributions characterizing the spatial distribution of the field. The resulting variables are input to discriminant analysis, to determine how well a flare-imminent photospheric magnetic field as defined on a daily basis, can be distinguished from a flare-quiet one.

2.5.2 Summary of Results

By considering both the magnitudes of the coefficients in an all-variable discriminant function and the results of a "step-up" procedure for determining the best m-variable discriminant function (12), we find that only a few variables are needed to extract the majority of the predictive power of the photospheric parameters. For example, the three-variable combination of the total magnetic flux, $\Phi_{\rm tot}$, the standard deviation of the magnetic shear angle along neutral lines, $\sigma(\Psi_{\rm NL})$, and the mean of the shear angle, $\bar{\Psi}$, are able to correctly classify 80.3% of the active regions in our sample. This is only about 1% less than simultaneously using all of the variables considered.

However, due to strong correlations among the parameters, many other three-variable combinations perform nearly as well. We find that there are a number of strongly correlated variables that

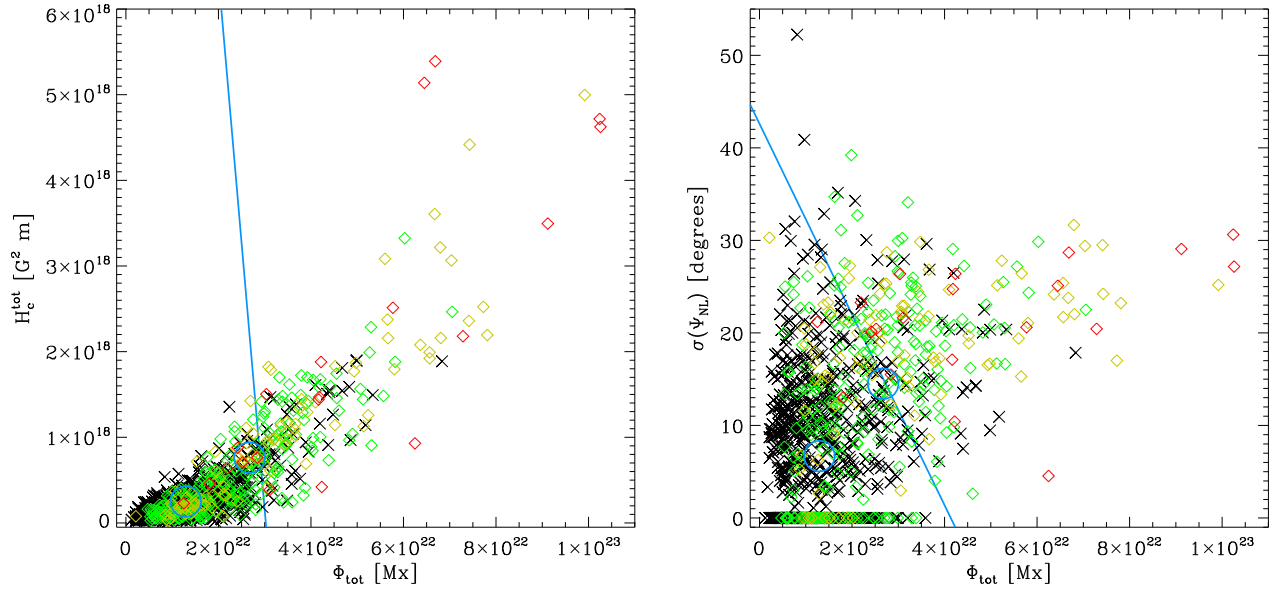

Figure 3: Examples of 2-variable discriminant functions for strongly correlated variables $\Phi_{\rm tot}$ and $H_c^{\rm tot}$ (left) and uncorrelated variables $\Phi_{\rm tot}$ and $\sigma(\Psi_{\rm NL})$ (right). Non-flaring regions are indicated by black crosses, while flaring regions are shown as colored diamonds, with the largest flare given by green for C-flares, yellow for M-flares and red for X-flares. The mean of each sample is shown as a blue circle, and the discriminant function is the blue line. There are a number of points with $\sigma(\Psi_{\rm NL}) = 0.0$ that are from regions where there are no well measured horizontal fields on the neutral line. The points with $\Phi_{\rm tot} \sim 10^{23}$ Mx are region NOAA AR 10486.

can be good predictors, including measures of the total flux, the total current, the total current helicity and the excess photospheric magnetic energy. Figure 3 illustrates the discriminant function for a pair of strongly correlated variables, and for a pair of uncorrelated variables. Combining strongly correlated variables adds little predictive power to considering either variable alone.

Although we have achieved a greater than 80% success rate, note that it is possible to correctly classify about 70% of the active regions by simply forecasting that nothing will ever flare, so the amount of additional information gained from the photospheric magnetic field is fairly small. Thus far it is assumed that the distribution of each of the variables is Gaussian, and that the flaring and non-flaring populations have equal covariance matrices. This results in a particularly simple form for the discriminant function. However, with the large sample size considered, it is shown that making a nonparametric estimate of the probability density function results in only slight improvements to the rate of correct classification. To improve upon the predictive capability, it seems likely that one must consider the evolution of the photospheric magnetic field or some characterization of the coronal magnetic field.

2.6 Probabilistic Forecasts from Daily Vector Magnetograms

Barnes, G., Leka, K.D., Schumer, E., Della-Rose, D. 2006, "Probabilistic Forecasting of Solar Flares from Discriminant Analysis of Vector Magnetogram Data", *Space Weather J.*, in preparation.

Abstract

Discriminant analysis is a statistical approach for assigning a measurement to one of two mutually exclusive groups. It has been adapted for use in solar flare forecasting to provide the probability that the measurement belongs to either group, where the groups correspond to solar active regions which are flare imminent and those that are flare quiet. The technique is demonstrated for a large database of vector magnetic field measurements obtained by the U. Hawai'i Imaging Vector Magnetograph. For one particular combination of variables characterizing the photospheric magnetic field, the results are compared to a Bayesian approach for solar flare prediction, and to the method employed by the U.S. National Oceanic and Atmospheric Administration (NOAA). A quantitative comparison is difficult as the present method provides active region (rather than whole-Sun) forecasts, and the database covers only part of one solar cycle, however, the performance of the present method appears comparable to the other approaches for M-class flares.

2.6.1 Summary of Results

To compare the results of discriminant analysis to other forecasting methods, such as a recent Bayesian approach (36; 37) and the approach based on the McIntosh classification scheme (24) used by NOAA's Space Environment Center, it is necessary to produce probabilistic forecasts instead of merely assigning a measurement to one of two categories. To do this, the probability that a measurement belongs to each of the two populations is made, based on an estimate of the probability density function, $\hat{f}$, at that point. Assuming that the *a priori* probability of membership in a population is proportional to the sample size, the probability that a measurement $\boldsymbol{x}$ belongs to a flaring region is given by

$$P_f(\mathbf{x}) = \frac{n_f f_f(\mathbf{x})}{n_f f_f(\mathbf{x}) + n_q f_q(\mathbf{x})}. \tag{2}$$

where n_j is the sample size, $f_j(\mathbf{x})$ is the probability density function for population j, and $j = f$ refers to the flaring population, while $j = q$ refers to the flare-quiet population. We have applied this probability forecasting technique to the same database used previously (19) for the best combination of three variables.

To evaluate the performance of the probability forecasts, the reliability plot (Fig. 4) and verification statistics (Table 3) are employed (37). These include considering the average over all observed active regions of the forecast probability, $\langle f \rangle$, and of the observations, $\langle x \rangle$ (where x is either one or zero depending on whether the region flared or was flare-quiet), as well as the average of the forecast probability over flaring regions, $\langle f | x = 1 \rangle$, and over flare-quiet regions, $\langle f | x = 0 \rangle$. These averages are supplemented by the mean absolute error,

$$\mathrm{MAE}(f, x) = \langle |f - x| \rangle, \tag{3}$$

and the mean square error,

$$\mathrm{MSE}(f, x) = \langle (f - x)^2 \rangle. \tag{4}$$

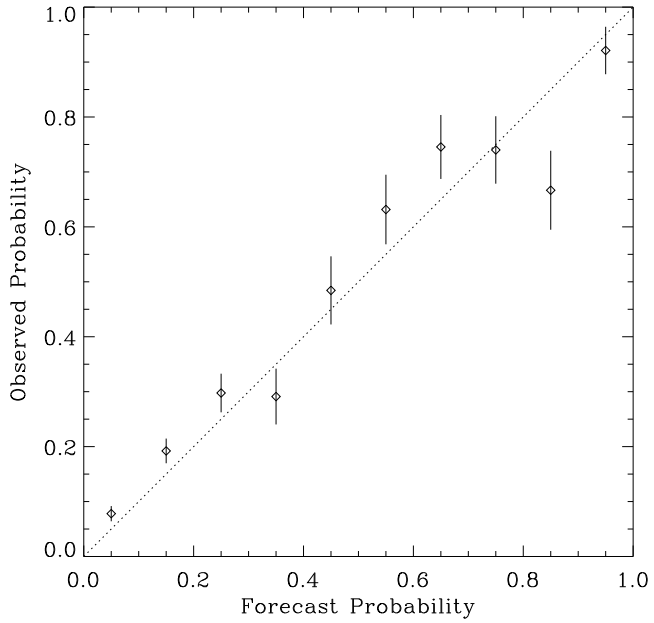

Figure 4: Reliability plot, in the same format as SEC. The forecast probabilities are divided into bins, and the observed probability for each bin is calculated based on the fraction of regions which did flare; error bars are estimated from the number of points in the bin. Perfect forecasts fall on the diagonal dotted line.

Table 3: Comparison of Verification Statistics for DA method with the SEC and Bayesian (37) Methods

	DA	Bayesian	SEC
$\langle f \rangle$	0.274	0.294	0.298
$\langle x \rangle$	0.296	0.262	0.262
$\langle f \vert x = 1 \rangle$	0.480	0.510	0.551
$\langle f \vert x = 0 \rangle$	0.187	0.217	0.208
MAE(f, x)	0.285	0.289	0.271
MSE(f, x)	0.150	0.143	0.139
SS(f, x)	0.279	0.258	0.262

Finally, the climatological skill score (see e.g., 30), defined by,

$$\begin{aligned} \mathrm{SS}(f,x) &= 1 - \mathrm{MSE}(f,x)/\mathrm{MSE}(\langle x \rangle, x) \\ &= 1 - \mathrm{MSE}(f,x)/\sigma_x^2, \end{aligned} \tag{5}$$

is calculated. The skill score indicates the improvement of the forecasts over a constant forecast given by the average. Positive scores indicate better performance, with a maximum score of one for perfect forecasting, while negative scores indicate worse performance than simply a uniform prediction.

Table 3 compares the verification statistics for the best three-variable combination (19) to the other approaches, albeit for somewhat different situations. The present method has similar errors to the other methods, and a slightly higher skill score, indicating that it performs comparably to

existing forecast methods.

The investigation into this transition to probabalistic forecasts and skill score tests was initiated as part of the requirements for a Master of Science degree in Applied Physics for Capt. Evelyn Schumer at the Air Force Institute of Technology. Capt Schumer successfully defended her dissertation and was awarded the degree in 2005 (35).

2.7 Spectropolarimetry and Magnetic Field Maps in the Chromosphere

> Metcalf, T.R., Leka, K. D., Mickey, D. L. 2006, "The Imaging Vector Magnetograph at Haleakalā IV: Observations of Chromospheric Magnetic Fields with Na D-1 line Spectropolarimetry", *Solar Physics*, in preparation.

Observing the solar magnetic field in the chromosphere has been a goal because the chromosphere is the layer where the field becomes force-free. That condition implies that $\boldsymbol{J} \times \boldsymbol{B} = \boldsymbol{0}$, *i.e.,* there are no cross-field currents. In this case, the determination of the force balance becomes straightforward, and the interpretation of single-height observations as related to measuring the twist component of the magnetic helicity, for example, is much simpler (as discussed in (20)).

Observing the solar magnetic fields in the chromosphere is, however, much more difficult than for the photosphere. The fields are generally weaker, the available spectral lines often have more difficult interpretation concerning the radiative transfer, and an acceptable signal-to-noise is more challenging to obtain. Nonetheless, based on early investigations (25), the Imaging Vector Magnetograph at U. Hawai'i/Mees Solar Observatory on Haleakalā was designed to be able to acquire data in chromospheric lines. Routine acquisition of the NaI D-1 line (589.6 nm, $g_{\rm eff} = 1.33$) began in late October 2003 and are continuing, due to the successful installation of a filter-wheel and a suitable prefilter in 2003.

While the analysis of IVM data from the photospheric FeI 630.25 nm line is fairly well understood (29; 14; 13), the chromospheric data from NaI is quite different. We found that measuring the scattered light for 589.6 nm using the algorithm developed for the photospheric data produces results of uncertain bearing on the final data product. The default instrumental setup has been modified for NaI observations in terms of the spectral sampling and the number of spectral repeats obtained for signal/noise considerations and to accommodate the width of this spectral line.

The inversion of the NaI spectropolarimetry to a magnetic field map is based on the "derivative method" (10), an appropriate method for this spectral line since the Doppler width is much greater than the magnetic broadening. Since the spectra are somewhat noisy, a "smoothing" approach was developed which uses the Milne-Eddington solutions to compute analytic spectra that match the data at the wavelength position of choice. At said wavelength, these computed spectra are then used to compute the wavelength-derivatives of the Stokes spectra for computation of the field by the "derivative method". The width of the NaI line implies that there is a significant variation in the height of formation with wavelength; even with the broad response function of the IVM, we demonstrate that different layers of the upper photosphere to upper chromosphere are sampled. The target wavelength for the inversion is isolated using a Gaussian weighting function; for the inversion, the Stokes parameters are weighted with a ratio of $1{:}\sqrt{2}/2$ for the unpolarized (I) to polarized (Q, U, V) spectra. Due to the broad spectral response of the IVM, the inversion is performed at 70mA to obtain a chromospheric magnetic field map, rather than the 68mA previously used (25; 21).

A thorough investigation was undertaken to develop the algorithm for fitting the polarimetric spectra, the weighting of both the selected wavelength and the Stokes parameters. This manuscript

is in preparation, but will encompass a thorough description of obtaining chromospheric magnetic field data from the IVM.

2.8 Measuring the Free Magnetic Energy in Solar Active Regions

Direct measure of the magnetic free energy using chromospheric magnetic field data should allow pertinent information to be obtained concerning an active region's capability to produce solar flares. We conducted the following investigations along these lines.

2.8.1 The Free Magnetic Energy of Super Active-Region 10486

Due to the geo-effective impact of super-active region NOAA AR10486, it was decided to publish the measurements of the free magnetic energy of this region as obtained by the IVM in a timely manner, even prior to the "method" paper described above.

Metcalf, T. R., Leka, K. D. and Mickey, D. L. 2005, "Magnetic Free Energy in AR10486 on October 29, 2003", *Astrophys. J. Letters*, **623**, L53.

Abstract

We calculate the total and the free magnetic energy for solar NOAA active region 10486 on 2003 October 29 using chromospheric vector magnetograms observed with the Imaging Vector Magnetograph at Mees Solar Observatory in the Na i l5896 spectral line. The magnetic energy is derived from the magnetic virial theorem using observations spanning the X10 flare that occurred at 20:39 UT. Although poor atmospheric seeing prevented us from discerning changes in the free energy associated with the flare, there was an unusually large amount of free magnetic energy in NOAA AR 10486: $(5.7 \pm 1.9) \times 10^{33}$ ergs, which is consistent with the very high level of activity observed in this active region. It is thus plausible that the extreme activity was powered by the magnetic free energy.

2.8.2 Improving the Algorithm for Measuring the Free Energy

Wheatland, M. S. and Metcalf, T. R. 2006, "An Improved Virial Estimate of Solar Active Region Energy", *Astrophys. J.*, **636**, 1151.

Abstract

The MHD virial theorem may be used to estimate the magnetic energy of active regions on the basis of vector magnetic fields measured at the photosphere or chromosphere. However, the virial estimate depends on the measured vector magnetic field being force-free. Departure from the force-free condition leads to an unknown systematic error in the virial energy estimate and an origin dependence of the result. We present a method for estimating the systematic error by assuming that magnetic forces are confined to a thin layer near the photosphere. If vector magnetic field measurements are available at two levels in the low atmosphere (e.g., the photosphere and the chromosphere), the systematic error may be directly calculated using the observed horizontal and vertical field gradients, resulting in an energy estimate that is independent of the choice of origin. If (as is generally the case) measurements are available at only one level, the systematic error may be approximated using the observed horizontal field gradients together with a simple linear force-free model for the vertical field gradients. The resulting "improved" virial energy estimate is independent of the choice of origin but depends on the choice of the model for the vertical field gradients, i.e., the value of the linear force-free parameter α. This procedure is demonstrated for five vector magnetograms, including a chromospheric magnetogram.

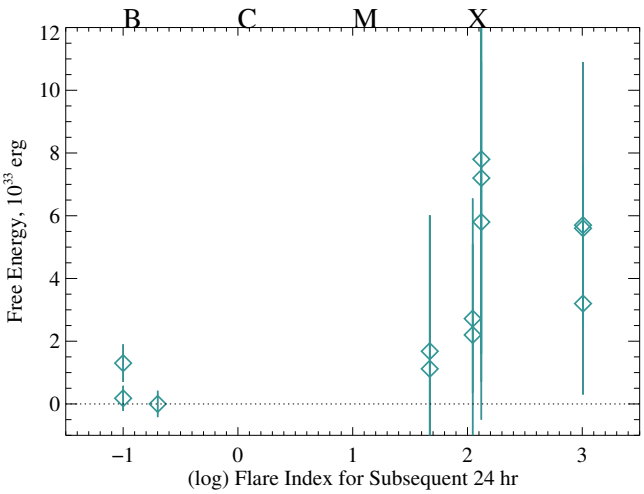

Figure 5: The magnetic free energy measured from maps of the chromospheric magnetic field derived from NaI data as a function of a flare productivity index. The latter is calculated effectively using a sum of the peak soft X-ray flux recorded by the GOES 1–8Å channel of the events which occurred in the 24hr following the magnetogram, and displayed on a logarithmic scale. This a preliminary plot, provided for demonstration only, illustrating the direction of our research using chromospheric magnetograms as related to flare production.

2.8.3 Free Energy as Statistically Related to Solar Flare Productivity

Leka, K.D. and Metcalf, T.R. 2006, "Solar Energetic Events and The Magnetic Free Energy of Active Regions", *Astrophys. J.*, in preparation.

A goal of obtaining observations of the solar chromospheric magnetic field is to measure the free magnetic energy available to power solar energetic events. We have observed previously that there can be measurable free energy in active regions (25; 28; 26) and that temporal variations in the free energy may be associated with energetic events (28; 26). The latter is an extremely difficult measurement to make and – while it was a goal for this contract – we have yet to acquire more than a single appropriate data set.

We are taking a different, statistical approach to investigate the basic relation between magnetic free energy and flare production. The IVM has, since 2003, acquired data in the chromospheric NaI line in both a time-sequence mode as well as a "survey" mode, building up a data base analogous to that for photospheric data (19). By comparing the free energy measured in an active region in such a "snapshot" mode with its flare productivity, we will confirm or deny the overall relevance of this investigative approach.

The data are being analyzed and the analysis will be completed under other contracts for which this science is also relevant. The causes for the delay are discussed elsewhere. A very preliminary version of results is shown here (Fig. 5). The flare productivity is a measure of the flare activity in the 24hr following the magnetogram, weighted by peak soft X-ray flux. The data are extremely sparse, so any correlation is just a hint. The goal is to obtain a statistically significant sample for publication, at least 100 different active regions, for analysis in this manner.

3 References

References

[1] Anderson, T. W.: 1984, *An Introduction to Multivariate Statistical Analysis*. New York: John Wiley.

[2] Barnes, G. and K. D. Leka: 2005, 'Photospheric Magnetic Field Properties of Flaring *vs.* Flare-Quiet Active Regions III: an Application of the Magnetic Charge Topology Analysis'. *Astrophys. J.* submitted.

[3] Barnes, G., K. D. Leka, E. A. Schumer, and D. Della-Rose: 2006, 'Probabilistic Forecasting of Solar Flares from Discriminant Analysis of Vector Magnetogram Data'. *Space Weather J.* in preparation.

[4] Barnes, G., D. Longcope, and K. D. Leka: 2005, 'Implementing a Magnetic Charge Topology Model for Solar Active Regions'. *Astrophys. J.* **629**, 561–571.

[5] Baum, P. J. and A. Bratenahl: 1980, 'Flux linkages of bipolar sunspot groups - A computer study'. *Solar Phys.* **67**, 245–258.

[6] Démoulin, P., J. C. Henoux, and C. H. Mandrini: 1994, 'Are magnetic null points important in solar flares?'. *Astron. Astrophys.* **285**, 1023–1037.

[7] Fan, Y. and S. E. Gibson: 2003, 'The Emergence of a Twisted Magnetic Flux Tube into a Preexisting Coronal Arcade'. *Astrophys. J. Letters* **589**, L105–L108.

[8] Gold, T. and F. Hoyle: 1960, 'On the Origin of Solar Flares'. *Mon. Not. R. Astron. Soc* **120**(2), 89–105.

[9] Gorbachev, V. S. and B. Somov: 1988, 'Photospheric vortex flows as a cause for two-ribbon flares - A topological model'. *Solar Phys.* **117**, 77–88.

[10] Jefferies, J., B. W. Lites, and A. Skumanich: 1989, 'Transfer of Line Radiation in a Magnetic Field'. *Astrophys. J.* **343**, 920–935.

[11] Kendall, M., A. Stuart, and J. K. Ord: 1983, *The Advanced Theory of Statistics*, Vol. 3. New York: Macmillan Publishing Co., Inc, 4th edition.

[12] Klecka, W. R.: 1980, *Disciminant Analysis*. Newbury Park: Sage Publications.

[13] Labonte, B.: 2004, 'The Imaging Vector Magnetograph at Haleakalā III: Effects of Instrumental Scattered Light on Stokes Spectra'. *Solar Phys.* **221**, 191–207.

[14] Labonte, B., D. L. Mickey, and K. D. Leka: 1999, 'The Imaging Vector Magnetograph at Haleakalā II: Reconstruction of Stokes Spectra'. *Solar Phys.* **189**, 1–24.

[15] Lau, Y.-T.: 1993, 'Magnetic Nulls and Topology in a Class of Solar Flare Models'. *Solar Phys.* **148**, 301–324.

[16] Leamon, R. J., R. C. Canfield, Z. Blehm, and A. A. Pevtsov: 2003, 'What is the Role of the Kink Instability in Solar Coronal Eruptions?'. *Astrophys. J. Letters* **596**, L255–L258.

[17] Leka, K. D. and G. Barnes: 2003a, 'Photospheric Magnetic Field Properties of Flaring *vs.* Flare-Quiet Active Regions I: Data, General Analysis Approach, and Sample Results'. *Astrophys. J.* **595**, 1277–1295.

[18] Leka, K. D. and G. Barnes: 2003b, 'Photospheric Magnetic Field Properties of Flaring *vs.* Flare-Quiet Active Regions II: Applying a Discriminant Function'. *Astrophys. J.* **595**, 1296–1306.

[19] Leka, K. D. and G. Barnes: 2005, 'Photospheric Magnetic Field Properties of Flaring *vs.* Flare-Quiet Active Regions III: Results from A Statistically Significant Number of "Daily" Magnetograms'. *Astrophys. J.* in preparation, see `http://www.cora.nwra.com/~leka/Preprints.html`.

[20] Leka, K. D., Y. Fan, and G. Barnes: 2005, 'On the Availability of Sufficient Twist in Solar Active Regions to Trigger the Kink Instability'. *Astrophys. J.* **626**, 1091–1095.

[21] Leka, K. D. and T. R. Metcalf: 2003, 'Active Region Magnetic Structure Observed in the Photosphere and Chromosphere'. *Solar Phys.* **212**, 361–378.

[22] Leka, K. D. and T. R. Metcalf: 2006, 'Solar Energetic Events and The Magnetic Free Energy of Active Regions'. *Astrophys. J. Letters* in preparation.

[23] Longcope, D. W. and I. Klapper: 2002, 'A General Theory of Connectivity and Current Sheets in Coronal Magnetic Fields Anchored to Discrete Sources'. *Astrophys. J.* **579**, 468–481.

[24] McIntosh, P. S.: 1990, 'The Classification of Sunspot Groups'. *Solar Phys.* **125**, 251–267.

[25] Metcalf, T. R., L. Jiao, A. N. McClymont, R. C. Canfield, and H. Uitenbroek: 1995, 'Is the Solar Chromosphere Magnetic Field Force-Free?'. *Astrophys. J.* **439**, 474–481.

[26] Metcalf, T. R., K. D. Leka, and D. L. Mickey: 2005, 'Magnetic Free Energy in AR10486 on October 29, 2003'. *Astrophys. J. Letters* **623**, L53–L56.

[27] Metcalf, T. R., K. D. Leka, and D. L. Mickey: 2006, 'The Imaging Vector Magnetograph at Haleakalā IV: Observations of Chromospheric Magnetic Fields with Na D-1 line Spectropolarimetry'. *Solar Phys.* in preparation.

[28] Metcalf, T. R., D. L. Mickey, B. J. LaBonte, and L. A. Ryder: 2002, 'The Magnetic Free Energy and a CME in AR8299'. In: *Multi-Wavelength Observations of Coronal Structure and Dynamics*, Vol. 13 of *COSPAR Colloquia Series*. pp. 249–252.

[29] Mickey, D. L., R. C. Canfield, B. J. LaBonte, K. D. Leka, M. F. Waterson, and H. M. Weber: 1996, 'The Imaging Vector Magnetograph at Haleakalā'. *Solar Phys.* **168**, 229–250.

[30] Murphy, A. H. and E. S. Epstein: 1989, 'Skill Scores and Correlation Coefficients in Model Verification'. *Mon. Weather Rev.* **117**, 572–582.

[31] Parnell, C. E., E. R. Priest, and L. Golub: 1994, 'The three-dimensional structures of X-ray bright points'. *Solar Phys.* **151**, 57–74.

[32] Pevtsov, A. A., R. C. Canfield, and T. R. Metcalf: 1995, 'Latitudinal Variation of Helicity of Photospheric Magnetic Fields'. *Astrophys. J. Letters* **440**, L109–L112.

[33] Priest, E. R. and T. G. Forbes: 1989, 'Steady magnetic reconnection in three dimensions'. *Solar Phys.* **119**, 211–214.

[34] Schrijver, C. J., H. J. Hagenaar, and A. M. Title: 1997, 'On the patterns of the solar granulation and supergranulation'. *Astrophys. J.* **475**, 328–337.

[35] Schumer, E. A.: 2005, 'Customization of Discriminant Function Analysis for Prediction of Solar Flares'. M.S. Thesis – AFIT.

[36] Wheatland, M. S.: 2004, 'A Bayesian Approach to Solar Flare Prediction'. *Astrophys. J.* **609**, 1134–1139.

[37] Wheatland, M. S.: 2005, 'A statistical solar flare forecast method'. *Space Weather J.* **3**, S07003.

4 Accomplishments: Technical Highlights

Algorithm development included research into new techniques as well as the optimization of both existing and new techniques for application to the appropriate data. Technical development was focused in the following areas.

4.1 Discriminant Analysis

The initial implementation of discriminant analysis, assuming populations with Gaussian probability distributions and equal covariance matrices, was generalized, first to allow for unequal covariance matrices, and then to include a nonparametric estimate of the probability density function. The use of nonparametric techniques means that no *a priori* assumptions need be made about the distribution function, making this a much more general approach, although extremely large sample sizes may be needed to accurately represent it.

In addition, the approach of discriminant analysis to classifying a new measurement as belonging to one of two populations was adapted to produce an estimate of the probability of belonging to each population. This adaptation allows for probability forecasting for solar flares, which in term enables comparison with existing forecasting techniques.

The code for the discriminant analysis consists of 42 programs written in IDL and Fortran, and is made available (see Appendix 6).

4.2 Magnetic Field Analysis

Methods were developed for the autonomous analysis of vector magnetic field data, considering both time-series data and the large set of single magnetograms. The former presented issues centered on the effects of atmospheric seeing and the sensitivity of ambiguity-resolution algorithms to minor changes in instrumental offsets. The latter presented challenges relating to the wide variety of morphologies and observing angle in addition to the effects of atmospheric seeing conditions. Code was optimized for speed and autonomy (no subjective intervention required by an operator). Additionally, flexibility was required to test limits and thresholds (noise rejection criteria, for example) and to modify and add new analysis parameters.

The code for the magnetic field analysis, both time-series and daily magnetogram datasets, consists of 60 routines written in IDL which also call a variety of routines in both the "IVM" and "MGRAM" code trees, described below. These are all made available (see Appendix 6).

4.3 Partitioning and the Coronal Topology for Time-Series Data

The partitioning of time series of photospheric magnetic field into flux concentrations was greatly improved by introducing a "reference" magnetogram. When treating each magnetogram in a time series separately, large fluctuations in the partitioning occur due to random noise, and particularly due to systematic changes in atmospheric seeing conditions. By minimizing the difference in partitioning between each magnetogram and the reference, the remaining evolution of the partitioning is primarily a result of real changes on the Sun.

The code for determining the topological properties of the coronal magnetic field was rewritten and optimized in Fortran, including making use of a Bayesian estimate for the domain flux, leading to improvements in speed or precision of more than 100. More than 220 routines in both Fortran and IDL were implemented for this analysis, and are made available (see Appendix 6).

4.4 Data Reduction and Inversion of Chromospheric Spectropolarimetry

The technical requirements to produce quantitative chromospheric magnetic field data from spectropolarimetric observations of the NaI D-1 line proved much more difficult than initially estimated. Preliminary approaches concerning the treatment of scattered light, the inversion of the spectra to produce a magnetic field map, and the treatment of the uncertainties for the calculation of the magnetic free energy all provided serious challenges. Due to these unforeseen setbacks, but also with the good fortune of continuing funding to work on these data, we are continuing these efforts and will cite this AFOSR funding for future publications based on the code development established here.

The code developed for the data reduction and inversion of the spectropolarimetry is part of the "IVM" data-reduction code tree. To obtain a vector field map of either photospheric or chromospheric data, the ambiguity in the transverse field must be resolved; the codes for this analysis and the calculation of the magnetic energy and related quantities are part of the "MGRAM" code tree. The "IVM" and "MGRAM" code trees, comprising 338 and 167 modules respectively, have been made available (see Appendix 6).

5 Additional Summaries

5.1 Significance to the Technical Field

In the original proposal we outlined the crucial guideline for conducting research into the possibility of solar flare prediction: a quantitative analysis of the state of the solar magnetic field with explicit tests of the null hypothesis. Our insistence that flare-quiet regions and epochs be tested and compared to flare-active regions and epochs has now been widely recognized by other research groups. The discriminant analysis method has also been recognized as a powerful tool, and we expect that this evaluation will become more so when Papers III,IV of our series appear in print. Our published papers have earned respectable citations in the very short time since they've appeared.

The use of chromospheric data is gaining acceptance as a "direction in which to head", however it is also recognized to be a very difficult task. It is also widely acknowledged in the solar physics community that our research is on the cutting edge, and that in pushing for this observational capability and working to ensure a quality, quantitative product, the scientific reward will be generous. Numerous other research groups have requested the chromospheric data for their own analysis. We are committed and funded to continue the refinement of the data reduction and analysis methods, providing data to the solar physics community once we are confident of the data quality, and publishing the results of our investigations in a timely manner.

5.2 Relationship to Original Goals

The following was the list of original goals and targeted deliverables for the contract:

1. Algorithms and code packages for manipulating and analyzing large sets of vector magnetic field data;
2. Novel applications of the Minimum Current Corona analysis and Discriminant Function analysis to time-series of photospheric vector magnetic field data;
3. A definitive, quantitative evaluation of the merit of using photospheric vector magnetic field data for solar energetic event prediction (or alternatively, a quantitative case *against* the use of photospheric data for this purpose);
4. A first attempt to address known shortcomings of photospheric vector field data, specifically the use of high time resolution *chromospheric* vector magnetic field data for evaluating the flaring capability of solar active regions.

We have succeeded in items #1, and 3 fully. For item #2 we modified the approach slightly to use the more tractable Magnetic Charge Topology analysis but have otherwise been successful; an investigation of the full MCC has now been funded by AFOSR, so work on this general topic will continue. Item #4 proved problematic to obtain in full, in part due to instrumental problems and in part due to the declining solar activity, thus our research approaches were modified. In this manner, we have (re)-designed relevant, productive studies to conduct with the resources and data available, as described above.

5.3 Relevance to the Air Force Mission

This research is driven by the need for the armed forces to be confident in their communications during high-risk times. Predicting the occurrence of a solar flare can be critical to today's warfighters, as – contrary to the few-days lag for the impact by Coronal Mass ejections – there is little if any lag time between the observation of the solar flare and the effect of its X-ray emission on communication technology.

We have investigated physics-based approaches to this specific area of solar flare prediction. While some of our results report a negative or less than useful prediction tool, we point out that a well-posed investigation which ends in a null result is extremely useful. We also have presented approaches that may in fact prove fruitful and should be tested further with larger-number statistics in a more applications-oriented situation.

5.4 Potential Applications to Technology Challenges

The algorithms developed for this contract utilize potential-field calculations with the argument that they represent the lowest-energy state of the model corona. As such, a lower bound can be calculated with MCT analysis and from which the free energy is calculated. For technology challenges, our position is that potential applications should be replaced with non-linear force-free extrapolations for a more realistic representation of the Sun.

5.5 Personnel Supported

Name	Location	Degree	Discipline	Involvement/Cost
In-House Personnel:				
K. D. Leka, P.I.	NWRA/CoRA	Ph.D.	Astronomy & Physics	0.33 FTE
Graham Barnes	NWRA/CoRA	Ph.D.	Physics & Astronomy	0.50 FTE
Thomas R. Metcalf	NWRA/CoRA[1]	Ph.D.	Physics	0.10 FTE
Subcontracts:				
Thomas R. Metcalf	Lockheed/Martin[2]	Ph.D.	Physics	0.10 FTE
Visitors/Collaborators:				
Dana Longcope	Montana State U.	Ph.D.	Applied Physics	no expenditure
Colin Beveridge	Montana State U.	Ph.D.	Mathematics	no expenditure
Capt. Evelyn Schumer	AFIT	M.S.	Applied Physics	no expenditure
Maj. Devin Della-Rose	AFIT	Ph.D.	Physics	no expenditure
Donald L. Mickey	U. Hawai'i	Ph.D.	Physics	no expenditure

[1] from 08/2005
[2] 2003 – 08/2005

5.6 Publications Citing this AFOSR Support (current and anticipated):

Published or submitted:

1. Leka, K.D. and Barnes, G. 2003, "Photospheric Magnetic Field Properties of Flaring Versus Flare-Quiet Active Regions. I. Data, General Approach, and Sample Results", *Astrophys. J.*, **595**, 1277.

2. Leka, K.D. and Barnes, G. 2003, "Photospheric Magnetic Field Properties of Flaring Versus Flare-Quiet Active Regions. II. Discriminant Analysis", *Astrophys. J.*, **595**, 1296.

3. Metcalf, T. R., Leka, K. D. and Mickey, D. L. 2005, "Magnetic Free Energy in AR10486 on October 29, 2003", *Astrophys. J. Letters*, **623**, L53.

4. Leka, K.D., Fan, Y. and Barnes, G. 2005, "On the Availability of Sufficient Twist to Trigger the Kink Instability", *Astrophys. J.*, **626**, 1091.

5. Barnes, G., Longcope, D. and Leka, K.D. 2005, "Implementing a Magnetic Charge Topology Model for Solar Active Regions", *Astrophys. J.*, **629**, 561.

6. Wheatland, M. S. and Metcalf, T. R. 2006, "An Improved Virial Estimate of Solar Active Region Energy", *Astrophys. J.*, **636**, 1151.

7. Barnes, G., and Leka, K.D. 2006, "Photospheric Magnetic Field Properties of Flaring Versus Flare-Quiet Active Regions III: Magnetic Charge Topology Models", *Astrophys. J.*, submitted.

8. Leka, K.D. and Barnes, G. 2006, "Photospheric Magnetic Field Properties of Flaring Versus Flare-Quiet Active Regions IV: Discriminant Analysis of a Statistically Significant Sample of Daily Photospheric Magnetograms", *Astrophys. J.*, to be submitted.

Anticipated:

1. Barnes, G., Leka, K.D., Schumer, E., Della-Rose, D. 2006, "Probabilistic Forecasting of Solar Flares from Discriminant Analysis of Vector Magnetogram Data", *Space Weather J.*, in preparation.

2. Metcalf, T.R., Leka, K. D., Mickey, D. L. 2006, "The Imaging Vector Magnetograph at Haleakalā IV: Observations of Chromospheric Magnetic Fields with Na D-1 line Spectropolarimetry", *Solar Physics*, in preparation.

3. Leka, K.D. and Metcalf, T.R. 2006, "Solar Energetic Events and The Magnetic Free Energy of Active Regions", *Astrophys. J.*, in preparation.

5.7 Interactions:

Our research group has been very visible at meetings, presenting our research to numerous technical/scientific audiences, as the lists below indicate. In addition, in recognition of our expertise, we have been called upon numerous times for invited seminars and colloquia.

5.7.1 Invited Lectures and Presentations:

In chronological order, presenter is in boldface:

1. March 2003 U. Montreal Department of Physics Invited Colloquium, *Are we there yet? The drive to understand and predict solar energetic events*, **K. D. Leka**.

2. July 2003, Invited talk for the Solar, Heliospheric and Interplanetary Environment (SHINE) meeting, Wailea, HI, *Applying Vector Magnetic Field Data to "Real Problems"*, **K. D. Leka**.

3. July 2003, Invited talk for the Solar, Heliospheric and Interplanetary Environment (SHINE) meeting, Wailea, HI, *Observing Vector Magnetic Fields*, **T. R. Metcalf**.

4. July 2003, Big Bear Solar Observatory Invited Colloquium, *What makes a flare? Determining the magnetic signature of a flaring photosphere*, **K. D. Leka**.

5. September 2003, Montana State University Physics Department (solar physics group) invited presentation, *Spectropolarimetry of active regions: what, how, and who cares?*, **K. D. Leka**.

6. December 2003, Invited Colloquium at the High Altitude Observatory, NCAR, *What Makes a Solar Flare? Determining the Photospheric Magnetic Signature of a Flaring Active Region.*, **K. D. Leka**.

7. March 2004, Invited Colloquium at UCBerkeley/Space Sciences Lab, *The Magnetic Free Energy in Active Regions*, **T. R. Metcalf**

8. March 2004, Invited talk for Solar MURI workshop, UCBerkeley/Space Sciences Lab, *Magnetic Charge Topology (MCT) Analysis of NOAA AR 8210*, **G. Barnes**

9. July 2004, Invited talk for the Solar, Heliospheric and Interplanetary Environment (SHINE) meeting, Big Sky, MT, *Chromospheric vs. Photospheric Vector Fields: Striking Similarities and Intriguing Differences*, **K. D. Leka**.

10. May 2005, Invited talk to the AGU/SPD meeting, New Orleans, LA, *Chromospheric Vector Magnetic Field Observations of Active Regions as Related to Energetic Events*, **K. D. Leka**.

11. July 2005, Invited poster presentation to the AFOSR Scientific Advisory Board, Arlington, VA, *Predicting Solar Flares using Solar Magnetic Field Data*, **K. D. Leka**.

12. September 2005, Invited Colloquium to U. Colorado Physics/LASP departments, *The Magnetic Free Energy in Active Regions*, **T. R. Metcalf**.

13. October 2005, Invited Colloquium to U. Colorado Physics/LASP departments, *Are We There Yet? The Journey to Understand and Predict Solar Energetic Events*, **K. D. Leka**.

5.7.2 Consultative and Advisory Functions:

1. **Leka, Barnes**: Served on the Committee for Masters in Science degree to Capt. E. Schumer, Air Force Institute of Technology.

2. **Leka**: October 2005, invited presentation to the NOAA/SEC forecasters, Boulder, CO, on present and future data availability of magnetic field maps, and their applicability for the forecast center.

5.7.3 Participation in and Presentations at Professional Meetings:

In chronological order, presenter is in boldface:

1. May 2003, NOAA/SEC Space Weather Week, Boulder, CO, contributed poster, *Photospheric Magnetic Field Properties of Flaring vs. Flare-Quiet Active Regions I: Data, General Approach, and Sample Results*, **K. D. Leka**, G. Barnes

2. May 2003, NOAA/SEC Space Weather Week, Boulder, CO, contributed poster, *Photospheric Magnetic Field Properties of Flaring vs. Flare-Quiet Active Regions II: A Magnetic Charge Topology Model and Statistical Results*, **G. Barnes**, K. D. Leka, D. W. Longcope.

3. June 2003, AAS/Solar Physics Division meeting, JHU/APL Greenbelt MD, contributed poster *Magnetic Field Properties of Flaring vs. Flare-Quiet Active Regions I: Data, General Approach, and Sample Results*, **K. D. Leka**, G. Barnes.

4. June 2003, AAS/Solar Physics Division meeting, JHU/APL, Greenbelt, MD, contributed poster *Photospheric Magnetic Field Properties of Flaring vs. Flare-Quiet Active Regions II: A Magnetic Charge Topology Model and Statistical Results*, **G. Barnes**, K. D. Leka, D. W. Longcope.

5. July 2003, Solar, Heliospheric and Interplanetary Environment (SHINE) workshop Wailea, HI contributed poster, *Photospheric Magnetic Field Properties of Flaring vs. Flare-Quiet Active Regions I: Data, General Approach, and Sample Results*, **K. D. Leka**, G. Barnes.

6. July 2003, Solar, Heliospheric and Interplanetary Environment (SHINE) workshop Wailea, HI contributed poster, *Photospheric Magnetic Field Properties of Flaring vs. Flare-Quiet Active Regions II: A Magnetic Charge Topology Model and Statistical Results*, **G. Barnes**, K. D. Leka D. W. Longcope.

7. March 2004, NASA/Living With a Star Workshop, Boulder, CO contributed talk *Magnetic Charge Topology (MCT) analysis of NOAA AR8210, May 1, 1998*, **G. Barnes**, D. W. Longcope, K. D. Leka.

8. March 2004, NASA/Living With a Star Workshop, Boulder, CO contributed poster *Photospheric Magnetic Field Properties of Flaring vs. Flare-Quiet Active Regions III: Discriminant Analysis of a Statistically Significant Database*, **K. D. Leka**, G. Barnes.

9. April 2004, NOAA/SEC Space Weather Week, Boulder CO, contributed poster *Photospheric Magnetic Field Properties of Flaring vs. Flare-Quiet Active Regions III: Discriminant Analysis of a Statistically Significant Database*, **K. D. Leka**, G. Barnes.

10. June 2004, AAS/Solar Physics Division meeting, Denver CO, contributed poster *Magnetic topology, flux emergence/reconnection and velocities from a magnetic charge topology model for NOAA active region 8210*, **G. Barnes**, D. W. Longcope, K. D. Leka.

11. June 2004, AAS/Solar Physics Division meeting, Denver CO contributed poster *Photospheric Magnetic Field Properties of Flaring vs. Flare-Quiet Active Regions III: Discriminant Analysis of a Statistically Significant Database*, **K. D. Leka**, G. Barnes.

12. December 2004, RHESSI/TRACE workshop, Sonoma, CA, contributed presentation *Twist, Kink, and other Contortions: On the Availability of Sufficient Twist in Active Regions to Trigger the Kink Instability*, **K. D. Leka**, Y. Fan, G. Barnes.

13. December 2004, RHESSI/TRACE workshop, Sonoma, CA, contributed presentation *The Magnetic Free Energy in Active Region 10486*, **T. R. Metcalf**, K. D. Leka, D. L. Mickey.

14. April 2005, NOAA/SEC Space Weather Week, Broomfield CO, contributed presentation, *Measuring the Magnetic Free Energy Available for Solar Activity*, **K. D. Leka**, T. R. Metcalf.

15. April 2005, NOAA/SEC Space Weather Week, Broomfield CO, contributed presentation, *Discriminant Function Analysis for Objective Prediction of Solar Flares*, **E. Schumer**, D. Della-Rose, K. D. Leka, G. Barnes.

16. May 2005, AGU/Solar Physics Division meeting, New Orleans, LA, contributed presentation *Another Piece of the Elephant: Chromospheric Vector Magnetic Field Measurements*, **K. D. Leka**, T. R. Metcalf, D. L. Mickey.

17. July 2005, SHINE workshop, Kona, HI Contributed presentation *Chromospheric Vector Magnetic Field Observations of Active Regions as Related to Energetic Events*, **K. D. Leka**, T. R. Metcalf, D. L. Mickey, G. Barnes.

5.7.4 Extended Scientific Visits to and From Other Laboratories

1. **Leka** to the University of Hawaii in July 2003 to consult with D. Mickey on the acquisition of data from the Imaging Vector Magnetograph.
2. **Leka** to Montana State University, September 2003, to work with Dr. Richard Canfield and students on IVM data reduction (paid for by NASA funding; however, collaborative discussions relevant to this contract were held with Dr. Dana Longcope).
3. **Barnes** to Montana State University, December 2003, to work with Dr. Dana Longcope on magnetic topology issues, including subtleties of MCT analysis for time-series data.
4. **Leka, Metcalf, Barnes** to U. California, Berkeley, Space Sciences Lab, March 2004 MURI workshop (Dr. George Fisher, P.I.). Leka and Barnes were serving as consultants for magnetic field data and extrapolation techniques, respectively, to the MURI team. Visit was paid for jointly by this contract and AFOSR F49620-02-1-0191 (Dr. Sarah Gibson, P.I.).
5. **E. Schumer**, to NWRA/CoRA from AFIT, June 2004, for consultation on probabilistic forecasting research.
6. **Barnes** to Montana State University, June – August 2005 to work with Dr. Dana Longcope on magnetic topology issues. Trip was primarily sponsored by a separate NASA contract, nonetheless the collaboration included topics relevant to this contract.
7. **Metcalf** to NWRA/CoRA from LMSAL, February and April 2005, to consult with Drs. Leka & Barnes concerning chromospheric data analysis.

5.7.5 Professional Activities (editorships, conference and society committees, *etc.*)

Leka Chair, NASA Peer Review Panel, Spring 2003

Leka NSO Director Review Committee, Spring 2003

Leka NSO user's committee 1997 – 2005

Metcalf SHINE 2004 workshop organizing committee, 2003–2004

Metcalf Living With a Star workshop scientific organizing committee, 2004

Leka Scientific Organizing Committee for 2006 IAU Symposium on 3-D Structure of Active Region Magnetic Fields, 2004 – 2005

Leka Chair, NSO user's committee 2005 – present.

Metcalf Boulder Solar Day scientific organizing committee, 2006

Leka, Barnes, Metcalf Numerous occasions serving as referee for peer-reviewed publications (*Solar Physics, Astrophys. J., Nature, Astron. & Astrophys.*) and proposal peer-review panels (NSF, NASA).

6 Appendix

The "MGRAM" code package has been made widely available for use in performing the ambiguity resolution for data from the IVM as well as from other instruments. The "IVM" code package is, in general, only narrowly distributed as it is very instrument-specific. The "MCT" code package is also available from Montana State University, through Dr. Longcope.

Given the large number of separate programs developed during this contract and used to analyze the data discussed in the scientific investigation, it is unreasonable to provide a full code listing as part of this report. Nonetheless, all codes and code packages referred to here are available at

`ftp://ftp.cora.nwra.com/pub/leka/data/AFOSR0019.tar.gz`.